Density inversion of selected microgravity anomalies using L_2-smoothing and minimum support focusing stabilizers

Ivan ZVARA [iD], Roman PAŠTEKA[*] [iD], Roland KARCOL [iD]

Department of Engineering Geology, Hydrogeology and Applied Geophysics,
Faculty of Natural Sciences, Comenius University,
Ilkovičova 6, 842 15 Bratislava, Slovak Republic,
e-mail: ivan.zvara@uniba.sk, roman.pasteka@uniba.sk, roland.karcol@uniba.sk

Abstract: Interpretation and inversion of microgravity anomalies belong to important tasks of near-surface geophysics, mostly in cavities detection in engineering, environmental and archaeological applications. One of the mostly used concepts of inversion in applied gravimetry is based on the approximation of the model space by means of 2D or 3D elementary sources with the aim to estimate their densities by means of the solution of a corresponding linear equation system. There were published several approaches trying to obtain correct and realistic results, which describe real parameters of the sources. In the proposed contribution we analyse the properties of two additional functionals, which describe additional properties of the searched solution – namely so-called L_2-smoothing and minimum support focusing stabilizers. For the inversion itself, we have used the regularized conjugate gradient method. We have studied properties of these two stabilizers in the case of one synthetic model and one real-world dataset (microgravity data from St. Nicholas church in Trnava). Results have shown that proposed algorithm with the minimum support stabilizer can generate satisfactory model results, from which we can describe real geometry, dimensions and physical properties of interpreted cavities.

Key words: gravimetry, interpretation, inversion, regularisation, cavities

1. Introduction

Precise gravity acceleration measurements are used in a variety of applications, from structural geology problems to resource exploration (e.g. *Hinze et al., 2013*). One can't omit microgravimetry as a very useful tool for detection of shallow objects (what are, technically, small scale subsurface density inhomogeneities as voids or cavities (e.g. *Pašteka et al., 2020*)). Inversion of gravity field data can give a better insight on subsurface image: the source's

---

[*]corresponding author: e-mail: roman.pasteka@uniba.sk

63

depth, its geometry and physical properties (density contrast). Because of that, it is a very active field of development (e.g. *Li and Krahenbuhl, 2015*). However, inversion suffers from many problems. From mathematical point of view, the solution of inversion is non-unique and it is instable (or does not exist at all) – in other words it is a typical ill-posed problem of mathematical physics (*Groetsch, 1993*).

The most troublesome is the ambiguity (non-uniqueness) that exists in any geophysical method, based upon a static potential field. It can be reduced by applying a priory information. In general, this additional information about the solution (constrain) can have geological or mathematical-physical character. In this contribution we will analyse properties of methods in this second group of constrains (math/phys). One of the mostly used concepts of inversion in applied gravimetry is based on the approximation of the model space by means of 2D or 3D elementary sources (points, lines, rectangular prisms...) with the aim to estimate their densities by means of the solution of a corresponding linear equation system (e.g. *Last and Kubik, 1983; Li and Oldenburg, 1998*). Here several methods have been developed for the incorporation of the mathematical-physical information into the expected solution: *Last and Kubik, (1983)* proposed a minimum support (MS) stabilizing functional and applied it to 2D inversion of gravity data, *Rudin et al. (1992)* developed total variation (TV) stabilizing functional and used it for satellite image inversion, *Li and Oldenburg (1998)* introduced the depth weighting function. Later *Bertete-Aguirre et al. (2002)* used modified total variation stabilizer for inverting 2D gravity data and *Portniaguine and Zhdanov (1999)* proposed minimum gradient support (MGS) stabilizer which improved MS functional. The TV, MS and MGS are all special kinds of focusing stabilizers. In some situations, like mineral exploration or as above mentioned cavities detection, it is crucial to detect sharp boundaries between target source and host rock. However, the result obtained by using a focusing stabilizing functional highly depends on the right choice of the focusing parameter. *Zhao et al. (2016)* have introduced exponential stabilizer which doesn't need the focusing parameter.

This contribution is focused on the possibilities of density inversion methods in the interpretation of microgravity anomalies, caused by subsurface cavities – represented by e.g. crypts in archaeological prospection. There exist a variety of geophysical methods, used in near-surface and archaeological

64

applications, mostly DC geoelectrical methods, Ground Penetrating Radar (GPR) and shallow seismic methods (e.g. *Clark, 1990; Putiška et al., 2012; Brixová et al., 2018*). Microgravity method can contribute to this kind of detection (mostly cavities) – often in urban environments for archaeological applications, where only selected geophysical methods can be used (*Mrlina et al., 2005; Panisova et al., 2012, 2013*). In the process of interpretation of local negative anomalies, we use different quantitative methods (a short overview can be found in *Pašteka et al., 2020*). Among them density inversion methods became more and more popular in the last decade (e.g. *Zhao et al., 2016; Rezaie et al., 2017*), which is also the topic of this presented study. At first, we analyse the results from synthetic tests with different focusing stabilizers incorporated in the regularized conjugate gradient (RGC) method (*Zhdanov, 2002*) and then we choose the most suitable one for inverting gravity data from St. Nicholas church in Trnava (SW Slovakia).

2. Methodology

The model space is divided into a regular system of rectangular cells (2D or 3D rectangular prisms). The Cartesian coordinate system is adopted – positive part of the vertical axis z is oriented downward. The vertical component (V_z) of the gravitational attraction vector is then given by (e.g. *Karcol, 2018*):

$$V_z(x,z) = G \iint\limits_{\xi \ \zeta} \sigma(\xi,\zeta) \, \frac{(\zeta - z)}{(\xi - x)^2 + (\zeta - z)^2} \, \mathrm{d}\xi \, \mathrm{d}\zeta \qquad \rightarrow \text{2D case}, \qquad (1)$$

$$V_z(x,y,z) = G \iiint\limits_{\xi \ \eta \ \zeta} \frac{\sigma(\xi,\eta,\zeta)\,(\zeta - z)}{\left[(\xi - x)^2 + (\eta - y)^2 + (\zeta - z)^2\right]^{\frac{3}{2}}} \, \mathrm{d}\xi \, \mathrm{d}\eta \, \mathrm{d}\zeta \qquad (2)$$

$$\rightarrow \text{3D case},$$

where the Greek letters are related to the mass element, Latin letters stand for the position of the calculation point, σ is density function and G is Newton's gravitational constant. The solutions of previous integrations for the constant density are:

$$V_z(x, z) = G\sigma \left[2\left(\zeta - z\right) \arctan \frac{(\xi - x)}{(\zeta - z)} + \right.$$
$$\left. + (\xi - x) \ln\left[(\xi - x)^2 + (\zeta - z)^2\right] \right]_{\xi_1,\zeta_1}^{\xi_2,\zeta_2} \quad \rightarrow \text{ 2D case,} \tag{3}$$

$$V_z(x, y, z) = G\sigma \left[(\zeta - z) \ln[(\eta - y) + R] + (\eta - y) \ln[(\zeta - z) + R] - \right.$$
$$\left. - (\xi - x) \arctan \frac{(\eta - y)(\zeta - z)}{(\xi - x)\, R} \right]_{\xi_1,\eta_1,\zeta_1}^{\xi_2,\eta_2,\zeta_2} \quad \rightarrow \text{ 3D case,} \tag{4}$$

where $R = \sqrt{(\xi - x)^2 + (\eta - y)^2 + (\zeta - z)^2}$.

The software realization of the method is as follows: the effect of each prism is calculated for unity density with the help of equations (3) and (4), and then the multiplication with a density matrix (2D case) or a density array (3D case) is carried out (for each position of calculation point, of course) – i.e. a constant density of each cell/prism is used. Using matrix notation, the vector of the model space gravity field $\boldsymbol{d}$ is given by:

$$\boldsymbol{d} = \boldsymbol{A}\,\boldsymbol{m}, \qquad \boldsymbol{A} \in \mathcal{R}^{N \times M},\ \boldsymbol{d} \in \mathcal{R}^N,\ \boldsymbol{m} \in \mathcal{R}^M, \tag{5}$$

where $\boldsymbol{A} = a_{i,j}$, $i = 1, 2, \ldots, N$, $j = 1, 2, \ldots, M$ is the kernel matrix where $a_{i,j}$ is the contribution of jth prism to the gravity value on the ith observation point (according to equations (3) or (4) with unity density). The vector $\boldsymbol{m}$ (of size M) stands for model parameters (physical property of the single prism) and vector $\boldsymbol{d}$ (of size N) represents the calculated/measured data. The main objective of the inversion is to find density model which corresponds to the sub-surface density structure (geology) and which gravitational effect is in an acceptable fit (up to noise level) with measured data.

3. Density inversion

Gravity inverse problem is ill posed and suffers mainly from ambiguity. A typical way to solve ill posed problem is to use the regularization theory developed by *Tikhonov and Arsenin (1977)*. This method is based on minimization of the Tikhonov parametric functional:

$$P^\lambda(\boldsymbol{m}) = \varphi(\boldsymbol{m}) + \lambda S(\boldsymbol{m}), \tag{6}$$

where $\varphi(\boldsymbol{m})$ is the misfit functional between observed data and computed field, λ is regularization parameter and S is a stabilizing functional (stabilizer). In general, there are different stabilizers, each producing different result. Basically, we can divide the stabilizers into two groups: smoothing and focusing. The smoothing inversion algorithms are based on a minimum norm stabilizing functional such as L_1 and L_2 norms:

$$S_{L_1(m)} = \|\boldsymbol{m}\|_{L_1}^2 = (\boldsymbol{m},\boldsymbol{m})_{L_1}, \quad S_{L_2(m)} = \|\boldsymbol{m}\|_{L_2}^2 = (\boldsymbol{m},\boldsymbol{m})_{L_2}. \tag{7}$$

These types of inversion produce "smooth" solutions where sharp boundaries of the source are not developed. However, a lot of cases requires the presence of such sharper boundaries, for example the step change in density represents the cavity's edges in microgravity surveys for archaeological purposes. To achieve a sharp result, we can use stabilizing functional producing compact solutions, such as total variation (TV), minimum support (MS) or minimum gradient support (MGS) functional. Different stabilizers are expressed in Table 1.

Table 1. Comparison of different stabilizer equations. Coefficient ε also known as focusing parameter is very small positive number to avoid singularities where $\boldsymbol{m} = 0$.

Method	Stabilizer	Author
TV	$S_{\text{TV}}(\boldsymbol{m}) = \int\limits_V \sqrt{\|\nabla\boldsymbol{m}(\boldsymbol{r})\|^2 + \varepsilon^2}\, \mathrm{d}V$	*Acar and Vogel (1994)*
MS	$S_{\text{MS}}(\boldsymbol{m}) = \int\limits_V \dfrac{(\boldsymbol{m} - \boldsymbol{m}_{\text{apr}})^2}{(\boldsymbol{m} - \boldsymbol{m}_{\text{apr}})^2 + \varepsilon^2}\, \mathrm{d}V$	*Last and Kubik (1983)*
MGS	$S_{\text{MGS}}(\boldsymbol{m}) = \int\limits_V \dfrac{\nabla\boldsymbol{m}\cdot\nabla\boldsymbol{m}}{\nabla\boldsymbol{m}\cdot\nabla\boldsymbol{m} + \varepsilon^2}\, \mathrm{d}V$	*Portniaguine and Zhdanov (1999)*

In this work we select a minimum support functional (*Last and Kubik, 1983*), but we have tested also different stabilizers in synthetics inversion, where authors suggested seeking a source distribution with the minimum volume (compactness) to explain the anomaly. Parameter ε is used in many focusing stabilizers and is called a focusing parameter, needed to avoid singularity in case $\|\boldsymbol{m}\| = 0$. The focusing parameter also controls sharpness of the model. If the focusing parameter is set too small (values close to zero), the final model will be sharp. Larger values lead to smoother models.

The regularization parameter λ describes the trade-off between the best fitting and most reasonable stabilization. If selected λ is too small, the minimization of the Tikhonov parametric functional $P^\lambda(\boldsymbol{m})$ is equivalent to the minimization of the misfit functional and so there is a weak regularization, which could result in an unstable (incorrect) solution. When λ is too large, the minimization of the parametric functional $P^\lambda(\boldsymbol{m})$ is equivalent to the minimization of the stabilizing functional $S(\boldsymbol{m})$, which will force the solution to be closer to the *a priori* model. Vector $\boldsymbol{m}_{\mathrm{apr}}$ is an a priori model (given by user) – if not provided, then it is set to be a zero vector. In some cases, the stabilizing functional can increase from iteration to iteration. *Zhdanov (2002)* proposed to damp the regularization parameter proportionally to the increase of the stabilizing functional to assure convergence of parametric functional to the global minimum as follows:

$$\lambda_k = \lambda_1 q^{k-1}, \quad k = 1, 2, 3, \ldots, \quad q \in (0.5, 0.9). \tag{8}$$

We applied the regularized conjugate gradient method (RCG) (*Portniaguine and Zhdanov, 1999*) to search for the optimal solution, see Appendix A for a brief description of this algorithm.

4. Synthetic model

The synthetic model consists of two bodies (2D rectangular prism to represent buried elongated crypts) embedded beneath surface with zero background density, see Fig. 1 for model's scheme. The density contrast of the left-hand prism (black) is $-2\,\mathrm{g \cdot cm^{-3}}$, what represents empty (not watered) cavity. The second (right-hand) prism (grey) has the differential density $-1\,\mathrm{g \cdot cm^{-3}}$, what can mean that cavity is filled with some host material (light debris or water). The top of both prisms is placed in $-0.75\,\mathrm{m}$ below the surface.

The gravity data were computed along a perpendicular profile, with sample spacing 0.05 m, on the surface using (3) with the 5% uncorrelated Gaussian noise. Model space was discretized into $16\,000$ (200×80) 2D rectangular prisms. The inverse problem has been solved for two different stabilizers using RCG method: the L_2 stabilizer (S_{L_2}) and the minimum support (MS) stabilizers were used for inversion of synthetic data with the proposed inversion method. For the inversion we used a custom program *zInv* (programed
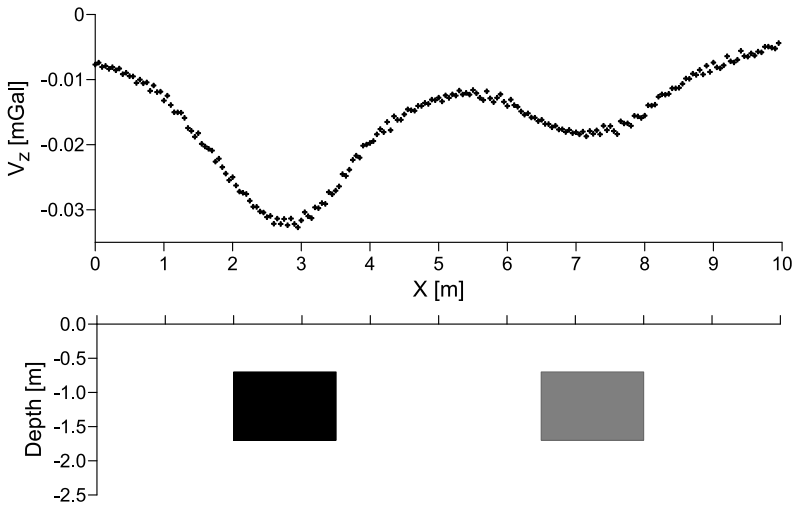
Fig. 1. The scheme and input field for the synthetic test. The black rectangle (left-hand): density $-2\,\mathrm{g}\cdot\mathrm{cm}^{-3}$, the grey rectangle (right-hand): density $-1\,\mathrm{g}\cdot\mathrm{cm}^{-3}$.

in the language C#), which has no option to calculate the regularization parameter using the L-curve (*Lawson and Hanson, 1974; Hansen, 1992*) – only option available is the trial and error method (the same for focusing parameter). The initial value of the regularization parameter λ for this model was selected as $4\cdot 10^{-7}$ and the focusing parameter ε as 0.9. The number of used iterations was 320.

The recovered models show strong difference between the smooth and focused inversion, see Fig. 2. The L_2 inversion produce more smooth result with a density range from 0 to $-1\,\mathrm{g}\cdot\mathrm{cm}^{-3}$ from which we are unable to estimate the real density distribution, thus it is not possible to define cavities, on the other hand the geometry distribution of sources is acceptable and can provide useful information about the approximate shape of possible sources. The focused stabilizer MS produces more suitable solutions in terms of density and geometry distribution. MS stabilizer defines the acceptable width and height approximation of the modelled cavities. The density reaches $-2\,\mathrm{g}\cdot\mathrm{cm}^{-3}$ for the left-hand prism and for the right-hand prism density values are determined between $-0.9\,\mathrm{g}\cdot\mathrm{cm}^{-3}$ and $-1.4\,\mathrm{g}\cdot\mathrm{cm}^{-3}$. With a survey focused on cavities detection, the MS result indicates satisfactory position
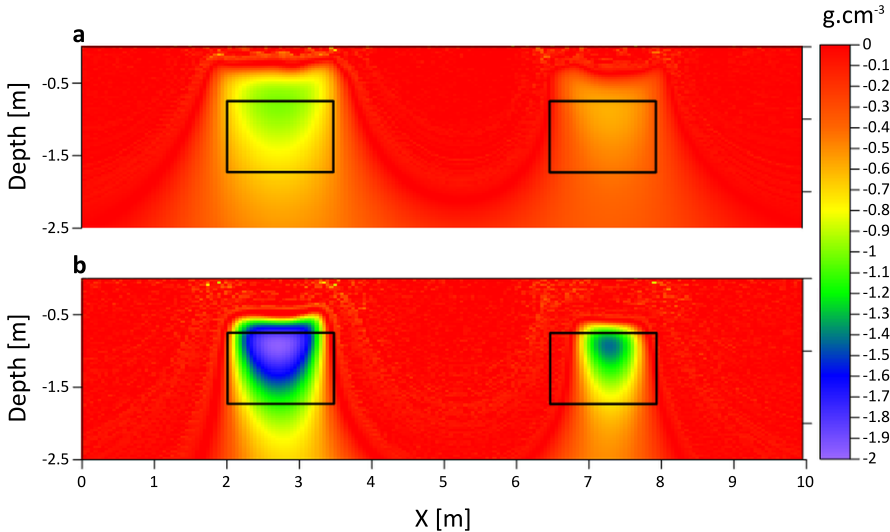
69

Fig. 2. Determined density models for different stabilizers using 2D density inversion with synthetic data: a) L_2 stabilizer, b) MS stabilizer.

and shape of sources (upper edges of the solutions are little bit shallower when compared with the real object, but this error is still acceptable).

5. Inversion of microgravity data from St. Nicholas church in Trnava

The georadar (GPR) and gravimetry survey was realized in 2006 in the interior of the St. Nicholas church in Trnava (*Terray, 2006a; Pašteka et al., 2007*). According to historical information there were indications about crypts buried below the church's central nave. A microgravimetry survey acquired (using Scintrex CG-5 gravimeter) 854 points in total (1 m × 1 m measuring grid) with the estimated measurement error ±0.007 mGal (*Pašteka et al., 2020*). Data were processed into residual Bouguer anomalies values (with removed planar background field) and gridded using kriging algorithm with cell size 0.1 m × 0.1 m. There are several important features on the final map, namely high-amplitude (from microgravimetry point of view) local minima, see Fig. 3.

Amplitudes of the 3 strongest anomalies, marked by D, E and F reach values between $-40\,\mu$Gal and $-50\,\mu$Gal. Such values can indicate the presence
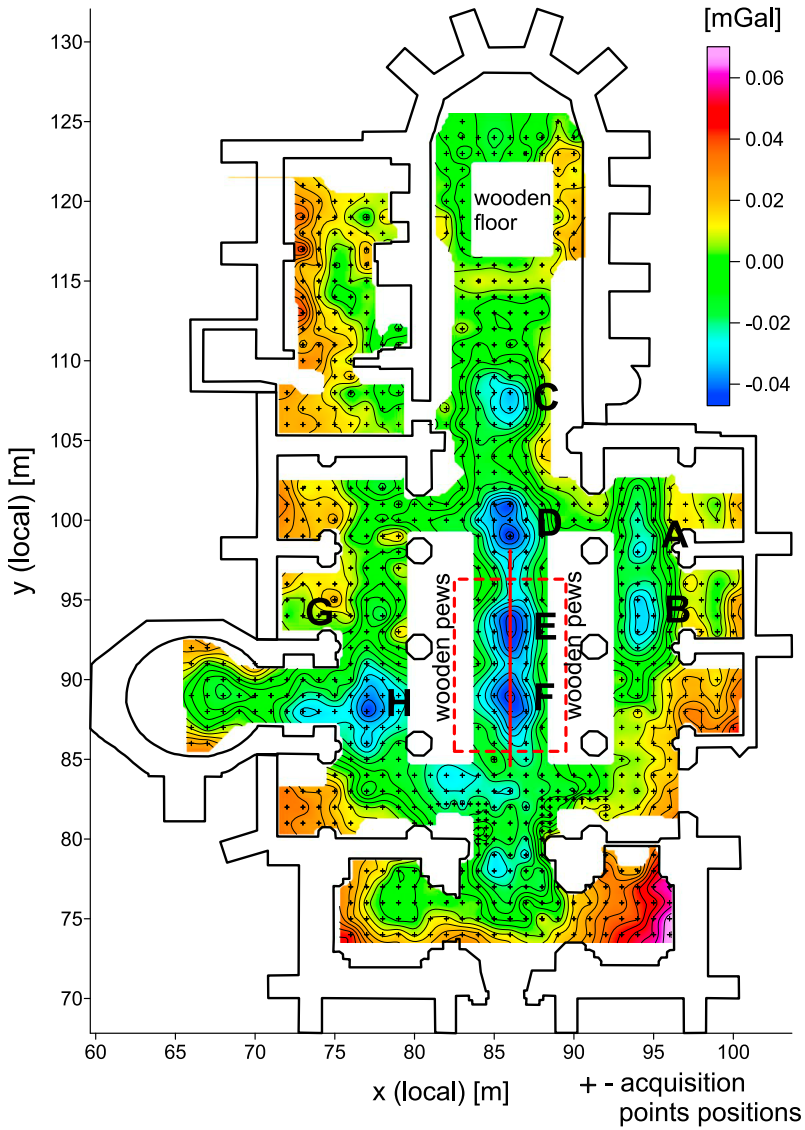
Fig. 3. The map of residual Bouguer anomaly from St. Nicholas church in Trnava (correction density: $1.80 \, \text{g} \cdot \text{cm}^{-3}$). Letters A – H show the detected negative gravity anomalies (possible connection with crypts). The 3D inversion's input anomalies are labelled E and F (highlighted by red dashed rectangle, position of GPR profile, led by their centre is highlighted by red abscissa).

of an empty, not collapsed or flooded cavity, most likely a crypt. Also results of the performed GPR measurements (*Terray, 2006a*) show all characteristic features of an existence of empty cavities (Fig. 4 – profile over E and F local minima).

Later, the geophysical survey was verified with a video inspection (*Terray, 2006b*) and with GPR combination it shows the actual geometry of the
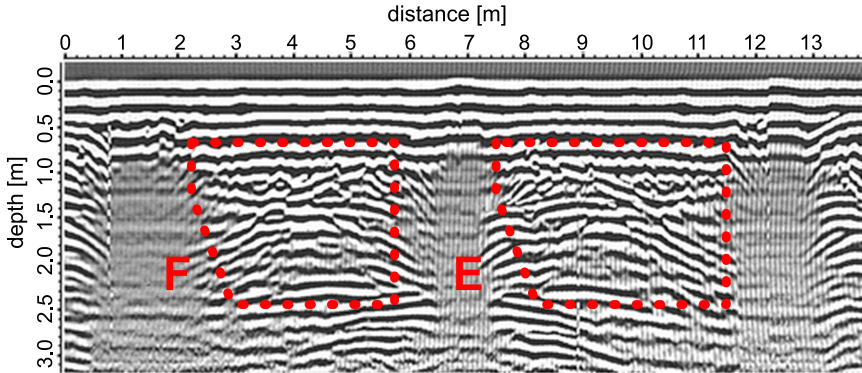
Fig. 4. Depth section from GPR measurements (adapted and modified from *Terray, 2006a*) along a profile, crossing the gravity anomalies E and F. Used velocity of EM waves for the conversion of time section into depth section was 0.1 m/ns.
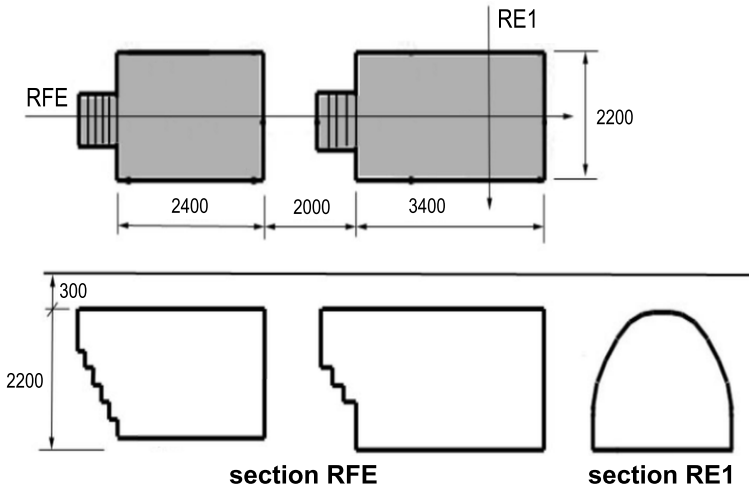
Fig. 5. Proposed shape and dimensions of crypts, determined from the results of performed video-inspection (adapted and modified after *Terray, 2006b*).

sources of the surveyed local minima E and F, which proved the presence of crypts and thus demonstrates the success of this combination method in archaeology (*Pašteka et al., 2007*). We can see the top boundary of the crypt located in 0.3 m depth from the surface and the total height of the crypt equals to 2.2 m, see Fig. 5. The length of the crypt E is estimated at 3.4 m. Both crypts have rectangle floor projection. Crypt F is of similar character as E with length of 2.4 m.

6. 2D results

To perform 2D inversion of gravity data over selected local minima (see Fig. 6 for detailed view), the subsurface of study area has been discretized into 20 000 (200 × 100) rectangular cells in x/y direction. For the inversion calculations, we have used again the custom program *zInv*. We applied RCG
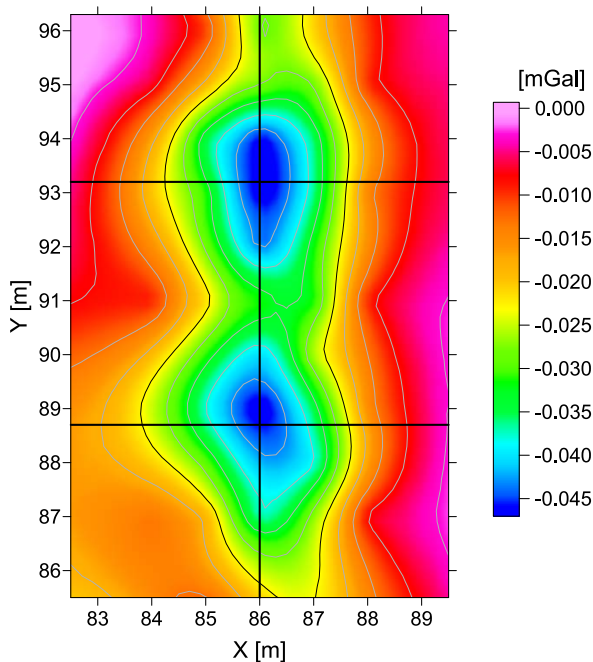

Fig. 6. Image of selected part of residual Bouger anomaly, with location of profiles used for 2D and 3D inversion (part of the acquired field – from the red dashed rectangle in Fig. 3).

inversion with two different stabilizers to show effectiveness of focused and smooth stabilizers in microgravimetry survey. 2D inversion was made in one YZ vertical slice and two XZ vertical slices (Figs. 7 and 8). The initial value of the regularization parameter λ in this case was set at 10^{-6} and the focusing parameter ε at 0.1 (the number of iterations used was 270). For MS stabilizer the 2D inversion result indicates that the depth of the top boundary of the crypt E is 0.8m and the bottom depth boundary is located at 2.6m below the surface. The solution length is 2.4m and height is 1.8m, although the shape of anomaly E is slightly deformed (Fig. 7). The density of this anomalous object reaches values between -1.3 g$\cdot$cm^{-3} and -2 g$\cdot$cm^{-3}. The depth of the top boundary of the crypt F is set at 0.7 m and the bottom depth boundary is 2.5 m below the surface. The resultant body has 2.1 m length and is 2 m high with density between -1.5 g $\cdot$ cm^{-3} and -2.1 g $\cdot$ cm^{-3}, see Fig. 7). From obtained densities we can state that the inverted bodies are not collapsed or flooded. In comparison, L_2 stabilizer produces more smoothed result, in YZ slice. The image shows two distinct bodies with slightly distorted geometry and density values from -0.6 g $\cdot$ cm^{-3} to -0.9 g$\cdot$cm^{-3} (Figs. 7 and 8). Results from both XZ slices present a better quality information for the interpretation of cavities. XZ slice at 93.2 m
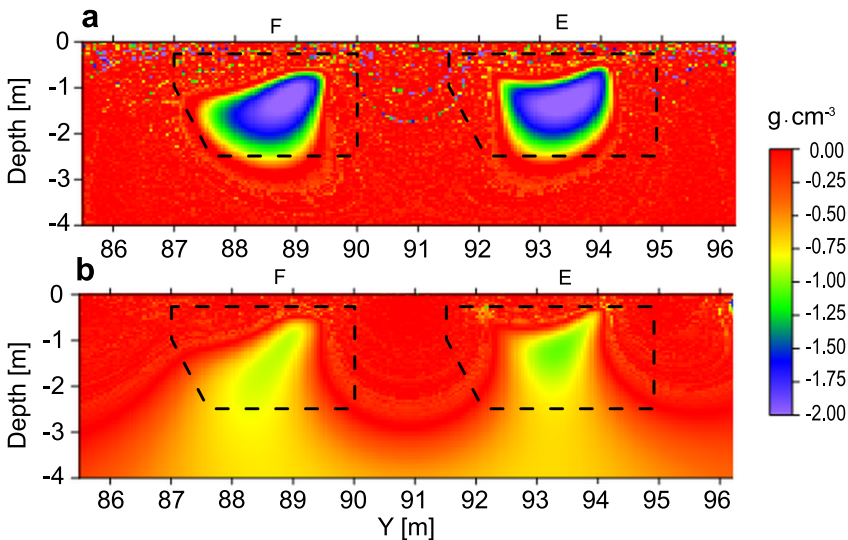

Fig. 7. Visualization of the 2D Inversion result comparing MS (a) and L_2 (b) stabilizing functional. The slice is made in YZ direction at $x = 86$ m.

(Fig. 8d) defines a body with $2\,\mathrm{m}$ length and $1.6\,\mathrm{m}$ height, which resembles the empty crypt below the surface.
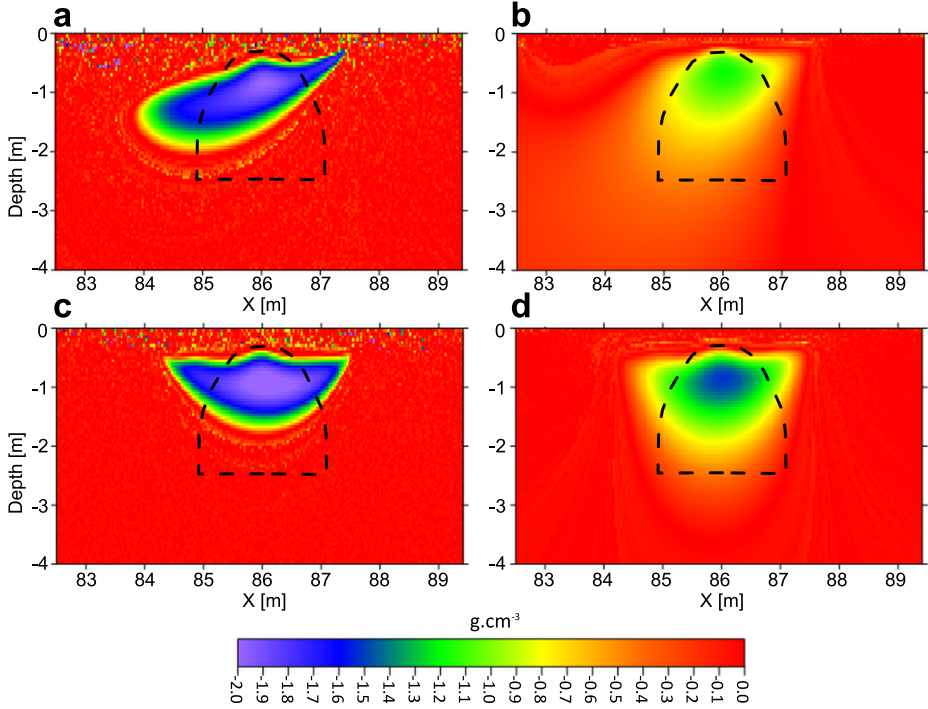

Fig. 8. 2D Inversion results comparing MS (a, c) and L_2 (b, d) stabilizing functional. The slices are made in XZ direction at $y = 88.7\,\mathrm{m}$ (a, b) and $y = 93.2\,\mathrm{m}$ (c, d).

7. 3D results

The 3D inversion of gravity data was performed too, but due to the lack of computer memory the model area has been discretized only into $245\,000$ $(70 \times 70 \times 50)$ cells in x, y and z direction resulting in worse spatial slice quality. The initial value of the regularization parameter λ in this case was set at 10^{-6} and the focusing parameter ε at 0.1 (the number of iterations used was 200). As expected, the results for L_2 stabilizer produced more smoothed images with not very sharp boundaries and shallower position (Fig. 9). The ceiling starts at $0.3\,\mathrm{m}$ and the bottom level ends in $1.2\,\mathrm{m}$, which doesn't describe the true geometry of crypts, although the algorithm
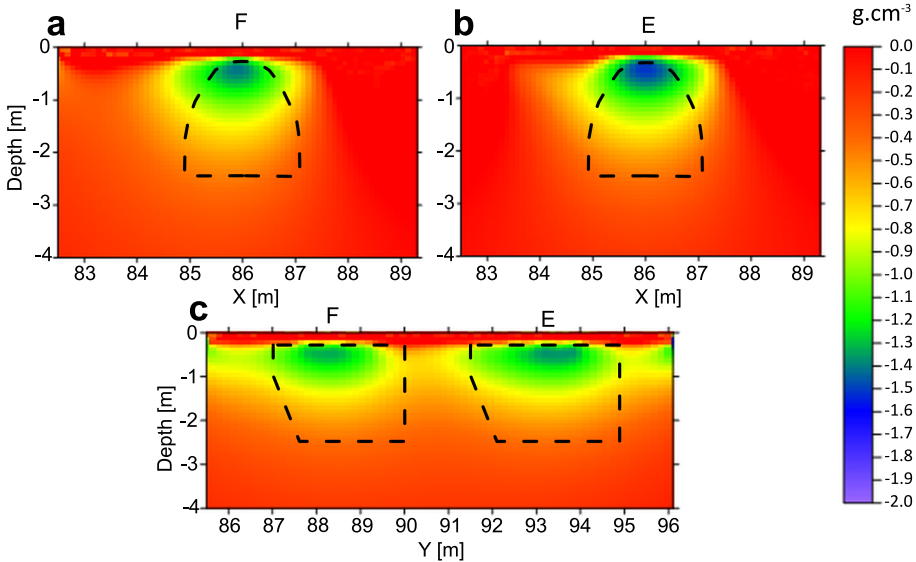
Fig. 9. 3D Inversion result for the L_2 stabilizer for two XZ slices (a, b) and one YZ slice (c) located at same coordinates as in 2D case.

produced an image with two distinct bodies. Such kind of information alone can later help other geophysical methods in interpretation, for instance it can represent an additional information to the GPR interpretation.

The results from the MS stabilizer clearly indicate the presence of 2 objects with densities similar to empty (not watered) crypts (Fig. 10). Width of both retrieved bodies is 3 m and height is approximately 2 m. However, with the applied discretization, the received XZ and YZ inversion results have a stronger "pixel-pattern" than in 2D case.

Comparing the video inspection image of the crypts (*Terray, 2006b*) with the inversion result we came to conclusion that the inversion produces acceptable result and we are able to estimate with good certainty that there are empty cavities under the surface (Fig. 11).

We can also make comparison between the results from 2D and 3D inversion of real-world gravity data. It shows that even when it is applied to anomalies of 3D character, the 2D inversion provide sufficient results. It is probably the effect of different model sizes in both cases, the 3D inversion requires a large amount of memory to process and store data, in many cases it is almost impossible to achieve the same resolution as in 2D
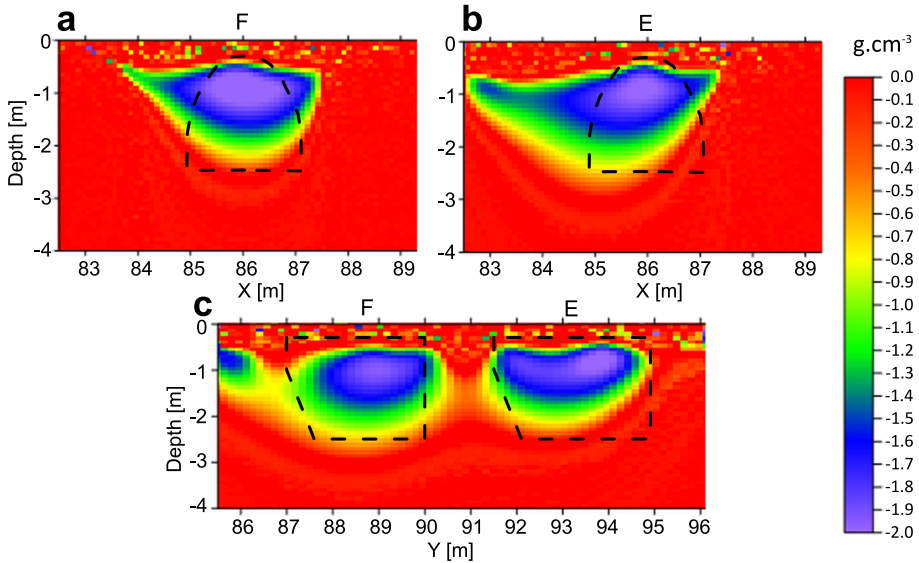
Fig. 10. 3D Inversion result for MS stabilizer for two XZ slices (a, b) and one YZ slice (c) located at same coordinates as in 2D case.

inversion. However, the result of 2D inversion places the anomalous bodies slightly deeper. In the case of 3D inversion, the anomalous bodies in vertical XZ slice are less deformed and their geometry is closer to real character of
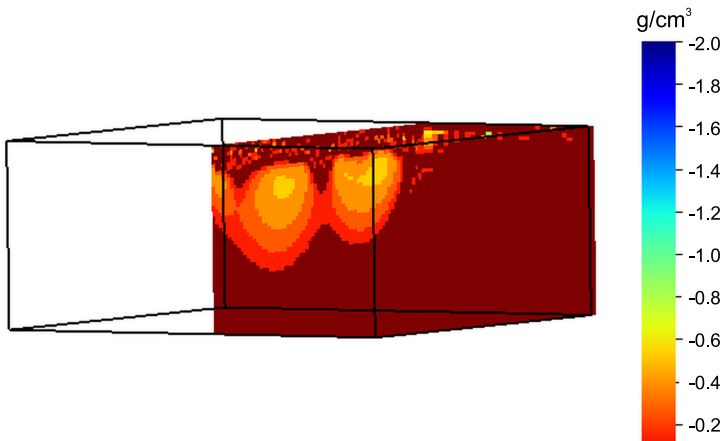

Fig. 11. Visualization of the 3D inversion result for the MS stabilizer (selected anomalies E and F from St. Nicholas church in Trnava).

crypts (Fig. 5). Generally, 3D inversion should give a better resolution and details in the resulting models. But 3D inversion is, in itself, more time and computation power consuming than 2D inversion, which made it time difficult to fine-tune parameters sufficiently.

8. Conclusions

The inverse solution of gravity data can determine the subsurface density distribution. From obtained results we can tell that inversion applied in archeogeophysics is a very helpful tool for determination of anomalous source geometry and density distribution. Because of the nature of some archaeological anomalies (isolated objects) it is suitable to use the minimum support (MS) focusing stabilizer, which yields models with sharp edges. Note that the stabilizing functional is highly dependent on the choice of correct focusing parameter, which can be calculated with help of various statistical methods; in our case with the trial and error method (with typical values from the interval $\langle 0.1, 0.9 \rangle$).

The robustness of the proposed algorithm has been proved by the synthetic model and a real gravity dataset from St. Nicholas church in Trnava. Inversion results can tell us a lot about the fill of the anomalous source – the obtained densities are close to the differential densities of an empty cavity (with the MS focusing stabilizer), in our case to the value $-2 \text{ g} \cdot \text{cm}^{-3}$. In the case of St. Nicholas church in Trnava, the performed 3D inversion (with the MS focusing stabilizer) estimated height at 2.1 m with the top boundary 0.45 m under the surface and with length of 3.3 m for crypt E. For crypt F the height is estimated at 2 m starting with the top boundary 0.41 m and with length of 2.7 m. These results demonstrate that proposed algorithm can generate a satisfactory model, from which we can describe real geometry, dimensions and physical properties of interpreted cavities.

References

Acar R., Vogel C. R., 1994: Analysis of total variation penalty methods for ill-posed problems. Inverse Probl., **10**, 6, 1217–1229, `doi:10.1088/0266-5611/10/6/003`.

Bertete-Aguirre H., Cherkaev E., Oristaglio M., 2002: Non-smooth gravity problem with total variation penalization functional. Geophys. J. Int., **149**, 2, 499–507, `doi:10.1046/j.1365-246X.2002.01664.x`.

Brixová B., Mosná A., Putiška R., 2018: Applications of shallow seismic refraction measurements in the Western Carpathians (Slovakia): case studies. Contrib. Geophys. Geod., **48**, 1, 1-21, `doi:10.2478/congeo-2018-0001`.

Clark A., 1990: Seeing Beneath the Soil: Prospecting Methods in Archaeology. Bathsford, 196 p.

Groetsch Ch. W., 1993: Inverse problems in the mathematical sciences. Springer, 152 p.

Hansen P. C., 1992: Analysis of discrete ill-posed problems by means of the L-curve. SIAM Rev., **34**, 4, 561–580, `doi:10.1137/1034115`.

Hinze W. J., von Frese R. R. B., Saad A. H., 2013: Gravity and Magnetic Exploration. Principles, Practices, and Applications. Cambridge University Press, 512 p.

Karcol R., 2018: The gravitational potential and its derivatives of a right rectangular prism with depth-dependent density following an n-th degree polynomial. Studia Geophys. et Geod., **62**, 3, 427–449, `doi:10.1007/s11200-017-0365-7`.

Last B. J., Kubik K., 1983: Compact gravity inversion: Geophysics, **48**, 6, 713–721, `doi:10.1190/1.1441501`.

Lawson C. L., Hanson R. J., 1974: Solving Least Squares Problems. Prentice-Hall, Englewood Cliffs, 305 p.

Li Y., Oldenburg D. W., 1998: 3-D inversion of gravity data. Geophysics **63**, 1, 109–119, `doi:10.1190/1.1444302`.

Li Y., Krahenbuhl R., 2015: Gravity and magnetic methods in mineral and oil & gas exploration and production. EAGE Publications bv, Education tour series, 155 p.

Mrlina J., Křivánek R., Majer A., 2005: Geophysical Survey in the St. Vitus Cathedral in Prague (Geofyzikální pr°uzkum k lokalizaci hrobky v katedrále sv. Víta v Praze). Castrum Pragense, **6**, 105–123 (in Czech, English abstract).

Panisova J., Pašteka R. Papčo J., Fraštia M., 2012: The calculation of building corrections in microgravity survey using close range photogrammetry. Near Surf. Geophys., **10**, 5, 391–399, `doi:10.3997/1873-0604.2012034`.

Panisova J., Fraštia M., Wunderlich T., Pašteka R., Kušnirák D., 2013: Microgravity and Ground-penetrating Radar Investigations of Subsurface Features at the St. Catherine's Monastery, Slovakia. Archaeol. Prospect., **20**, 3, 163–174, `doi:10.1002/arp.1450`.

Pašteka R., Terray M., Hajach M., Pašiaková M., 2007: Microgravity measurements and GPR technique in the search for medieval crypts: a case study from the St. Nicholas church in Trnava, SW Slovakia. Proceedings of the Archaeological Prospection 7th conference in Nitra, Štúdijné zvesti, **41**, 222–224.

Pašteka R., Pánisová J., Zahorec P., Papčo J., Mrlina J., Fraštia M., Vargemezis G., Kušnirák D., Zvara I., 2020: Microgravity method in archaeological prospection:

methodical comments on selected case studies from crypt and tomb detection. Archaeol. Prospect., **27**, 4, 415–431, `doi: 10.1002/arp.1787`.

Portniaguine O., Zhdanov M. S., 1999: Focusing geophysical inversion images. Geophysics, **64**, 3, 874–887, `doi: 10.1190/1.1444596`.

Putiška R., Nikolaj M., Dostál I., Kušnirák D., 2012: Determination of cavities using electrical resistivity tomography. Contrib. Geophys. Geod., **42**, 2, 201–211, `doi: 10.2478/v10126-012-0018-3`.

Rezaie M., Moradzadeh A., Kalateh A. N., 2017: Fast 3D inversion of gravity data using solution space priorconditioned lanczos bidiagonalization. J. Appl. Geophys., **136**, 42–50, `doi: 10.1016/j.jappgeo.2016.10.019`.

Rudin L. I., Osher S., Fatemi E., 1992: Nonlinear total variation based noise removal algorithms. Physica D: Nonlinear Phenomena, **60**, 1–4, 259–268, `doi: 10.1016/0167-2789(92)90242-F`.

Terray M., 2006a: Report from the georadar survey in the church of St. Nicholas in Trnava. Report, manuscript, Terra Inc. company Košice, 12 p. (in Slovak).

Terray M., 2006b: Report from the 2nd Phase of the georadar survey in the church of St. Nicholas in Trnava. Report, manuscript, Terra Inc. company Košice, 14 p. (in Slovak).

Tikhonov A. N., Arsenin V. Y., 1977: Solution of Ill-posed Problems. Washington: Winston & Sons, 258 p.

Zhao C., Yu P., Zhang L., 2016: A new stabilizing functional to enhance the sharp boundary in potential field regularized inversion. J. Appl. Geophysics, **135**, 356–366, `doi: 10.1016/j.jappgeo.2016.10.033`.

Zhdanov M. S., 2002: Geophysical Inverse Theory and Regularization Problems. Elsevier Science, Amsterdam, 633 p.

Appendix A – Regularized Conjugate Gradient (RCG) Algorithm

Inputs:

$\boldsymbol{A}$ – kernel matrix,

$\boldsymbol{d}$ – observed gravity data vector,

$\boldsymbol{m}$ – model parameters vector,

$(\boldsymbol{A} \in \mathcal{R}^{N \times M},\ \boldsymbol{d} \in \mathcal{R}^N,\ \boldsymbol{m} \in \mathcal{R}^M)$.

Variables:

r_n – residual vector at n^{th} iteration,

$\tilde{l}_0^\alpha$ – initialization of ascent direction vector,

$\tilde{l}_n^\alpha$ – ascent direction vector at n^{th} iteration (linear combination of the

steepest ascent at n^{th} step and the ascent's direction at the $(n-1)^{\text{th}}$ step),

l_n^α – direction of the steepest ascent,

k_n^α – coefficient of the step's optimum length,

β_n^α – conjugate direction coefficient to all previous directions,

m_{n+1} – updating model vector parameter.

Algorithm:

If $\boldsymbol{m}$ is not given then it is set to zero vector.

$r_n = A\,m_n - d\,,$

$l_n^\lambda = A^* W_d^2 (A\,m_n - d) + \alpha\,W_m^2 D_n\,,$

$\beta_n^\lambda = (l_n^\lambda l_n^\lambda)/(l_{n-1}^\lambda l_{n-1}^\lambda)\,,$

$\tilde{l}_n^\lambda = l_n^\lambda + \beta_n^\lambda\,\tilde{l}_{n-1}^\lambda\,,$

$\tilde{l}_0^\lambda = l_0^\lambda\,,$

$k_n^\lambda = (\tilde{l}_n^\lambda\,l_n^\lambda)/\{(W_d\,A\,\tilde{l}_n^\lambda, W_d\,A\,\tilde{l}_n^\lambda) + \alpha\,(W\,\tilde{l}_n^\lambda, W\,\tilde{l}_n^\lambda)\}\,,$

$m_{n+1} = m_n - k_n^\lambda\,\tilde{l}_n^\lambda\,.$

The inversion stops if the maximum number of iterations is reached or the target data misfit Root Mean Square (RMS) is reached, which is calculated as:

$$RMS = \sqrt{\frac{\sum\limits_{i=1}^{N}\left(\frac{d_i^{cal} - d_i^{obs}}{error_i}\right)}{N}}\,,$$

where d_i^{cal} and d_i^{obs} represent calculated (predicted) and observed data and $error_i$ is the estimated observation error. The calculated data are considered good when the value of RMS is less than some pre-determined tolerance, if RMS is too small it can indicate that the algorithm starts to fit the noise in the interpreted data-set. The target misfit is usually set at 1.